Local-field enhancement effect on the nonlinear optical response of gold-silver nanoplanets

T. Cesca,[1,*] P. Calvelli,[2] G. Battaglin,[2] P. Mazzoldi,[1] and G. Mattei[1,3]

[1]*Department of Physics, University of Padova, and CNISM, via Marzolo 8, I-35131 Padova, Italy*

[2]*Department of Molecular Sciences and Nanosystems, Ca' Foscari University of Venice, Dorsoduro 2137, I-30123 Venice, Italy*

[3]*giovanni.mattei@unipd.it*

[*]*tiziana.cesca@unipd.it*

Abstract: We report on the nonlinear optical properties of Au-Ag nanoplanets produced by ion implantation and irradiation in silica, experimentally investigated by means of the single beam z-scan technique. The measurements provided experimental evidence of the intense local-field enhancement effect theoretically demonstrated for these plasmonic nanosystems. In particular, this has a dramatic impact on their nonlinear absorption behavior and results in a tunable changeover from reverse saturable absorption to saturable absorption by slightly varying the pump intensity and in the possibility to activate and observe nonlinear phenomena of the electron dynamics otherwise unaccessible in the intensity range that can be employed to study these materials. Finally, for the nanoplanet configuration we found a dramatic decrease of the intensity-dependent absorption coefficient, which could be very promising for obtaining optical gain materials.

OCIS codes: (190.4400) Nonlinear optics, materials; (160.4236) Nanomaterials; (310.6628) Subwavelength structures, nanostructures; (310.3840) Materials and process characterization.

References and links

1. D. K. Gramotnev and S. I. Bozhevolnyi, "Plasmonics beyond the diffraction limit," Nat. Photon. **4**, 83–91 (2010).
2. S. Eustis and M. A. El-Sayed, "Why gold nanoparticles are more precious than pretty gold: Noble metal surface plasmon resonance and its enhancement of the radiative and nonradiative properties of nanocrystals of different shapes," Chem. Soc. Rev. **35**, 209 (2006).
3. K. M. Mayer and J. H. Hafner, "Localized surface plasmon resonance sensors," Chem. Rev. **111**, 3828–3857 (2011).
4. P. Genevet, J. Tetienne, E. Gatzogiannis, R. Blanchard, M. A. Kats, M. O. Scully, and F. Capasso, "Large enhancement of nonlinear optical phenomena by plasmonic nanocavity gratings," Nano Lett. **10**, 4880–4883 (2010).
5. S. Kim, J. Jin, Y. Kim, I. Park, Y. Kim, and S. Kim, "High-harmonic generation by resonant plasmon field enhancement," Nature **453**, 757–760 (2008).
6. G. Mattei, P. Mazzoldi, M. Post, D. Buso, M. Guglielmi, and A. Martucci, "Cookie-like Au/NiO nanoparticles with optical Gas-Sensing properties," Adv. Mater. **19**, 561–564 (2007).
7. J. N. Anker, W. P. Hall, O. Lyandres, N. C. Shah, J. Zhao, and R. P. Van Duyne, "Biosensing with plasmonic nanosensors," Nat. Mater. **7**, 442–453 (2008).
8. G. Mattei, P. Mazzoldi, and H. Bernas, "Metal nanoclusters for optical properties," in *Materials Science with Ion Beams*, H. Bernas, ed. (Springer-Verlag, Berlin Heidelberg, 2010), pp. 287–316.
9. A. L. Stepanov, "Nonlinear optical properties of implanted metal nanoparticles in various transparent matrixes: a review," Rev. Adv. Mater. Sci. **27**, 115–145 (2011).

#156046 - $15.00 USD Received 14 Oct 2011; revised 11 Nov 2011; accepted 13 Nov 2011; published 9 Feb 2012

10. R. A. Ganeev and A. I. Ryasnyansky, "Nonlinear optical characteristics of nanoparticles in suspensions and solid matrices," Appl. Phys. B **84**, 295–302 (2006).
11. Y. Guillet, M. Rashidi-Huyeh, and B. Palpant, "Influence of laser pulse characteristics on the hot electron contribution to the third-order nonlinear optical response of gold nanoparticles," Phys. Rev. B **79**, 045410 (2009).
12. U. Kreibig and M. Vollmer, *Optical Properties of Metal Clusters* (Springer-Verlag, Berlin Heidelberg, 1995).
13. G. Raschke, S. Brogl, A. S. Susha, A. L. Rogach, T. A. Klar, J. Feldmann, B. Fieres, N. Petkov, T. Bein, A. Nichtl, and K. Kürzinger, "Gold nanoshells improve single nanoparticle molecular sensors," Nano Lett. **4**, 1853–1857 (2004).
14. E. Cattaruzza, G. Battaglin, F. Gonella, G. Mattei, P. Mazzoldi, R. Polloni, and B. F. Scremin, "Fast third-order optical nonlinearities in metal alloy nanocluster composite glass: negative sign of the nonlinear refractive index," Appl. Surf. Sci. **247**, 390–395 (2005).
15. O. Plaksin, Y. Takeda, H. Amekura, and N. Kishimoto, "Radiation-induced differential optical absorption of metal nanoparticles," Appl. Phys. Lett. **88**, 201915 (2006).
16. M. Liu, P. Guyot-Sionnest, T. Lee, and S. K. Gray, "Optical properties of rodlike and bipyramidal gold nanoparticles from three-dimensional computations," Phys. Rev. B **76**, 235428 (2007).
17. E. Valentin, H. Bernas, C. Ricolleau, and F. Creuzet, "Ion beam "photography": Decoupling nucleation and growth of metal clusters in glass," Phys. Rev. Lett. **86**, 99 (2001).
18. P. Kluth, B. Johannessen, G. J. Foran, D. J. Cookson, S. M. Kluth, and M. C. Ridgway, "Disorder and cluster formation during ion irradiation of au nanoparticles in sio_2," Phys. Rev. B **74**, 014202 (2006).
19. R. Espiau de Lamaestre, H. Béa, H. Bernas, J. Belloni, and J. L. Marignier, "Irradiation-induced ag nanocluster nucleation in silicate glasses: Analogy with photography," Phys. Rev. B **76**, 205431 (2007).
20. P. Mazzoldi and G. Mattei, "Synthesis of metal nanclusters by using ion implantation," in *Metal Nanoclusters in Catalysis and Materials Science: The Issue of Size-Control*, B. Corain, G. Schmid, and N. Toshima, eds. (Elservier, Amsterdam, 2007), p. 281.
21. G. Mattei, G. De Marchi, C. Maurizio, P. Mazzoldi, C. Sada, V. Bello, and G. Battaglin, "Chemical- or Radiation-Assisted selective dealloying in bimetallic nanoclusters," Phys. Rev. Lett. **90**, 085502 (2003).
22. V. Bello, G. De Marchi, C. Maurizio, G. Mattei, P. Mazzoldi, M. Parolin, and C. Sada, "Ion irradiation for controlling composition and structure of metal alloy nanoclusters in SiO2," J. Non-Cryst. Solids **345-346**, 685–688 (2004).
23. G. Mattei, V. Bello, P. Mazzoldi, G. Pellegrini, C. Sada, C. Maurizio, and G. Battaglin, "Modification of composition and structure of bimetallic nanocluster in silica by ion beam irradiation," Nucl. Instrum. Meth. in Phys. Res. B **240**, 128–132 (2005).
24. G. Pellegrini, V. Bello, G. Mattei, and P. Mazzoldi, "Local-field enhancement and plasmon tuning in bimetallic nanoplanets," Opt. Express **15**, 10097–10102 (2007).
25. M. Sheik-Bahae, A. Said, T. Wei, D. Hagan, and E. V. Stryland, "Sensitive measurement of optical nonlinearities using a single beam," IEEE J. Quantum Electron. **26**, 760–769 (1990).
26. G. Battaglin, P. Calvelli, E. Cattaruzza, F. Gonella, R. Polloni, G. Mattei, and P. Mazzoldi, "Z-scan study on the nonlinear refractive index of copper nanocluster composite silica glass," Appl. Phys. Lett. **78**, 3953–3955 (2001).
27. R. Polloni, B. F. Scremin, P. Calvelli, E. Cattaruzza, G. Battaglin, and G. Mattei, "Metal nanoparticles-silica composites: Z-scan determination of non-linear refractive index," Journal of Non-Crystalline Solids **322**, 300–305 (2003).
28. S.-L. Guo, J. Yan, L. Xu, B. Gu, X.-Z. Fan, H.-T. Wang, and N. Ming, "Second z-scan in materials with nonlinear refraction and nonlinear absorption," J. Opt. A: Pure Appl. Opt. **4**, 504–508 (2002).
29. B. Gu, Y. Fan, J. Chen, H. Wang, J. He, and W. Ji, "Z-scan theory of two-photon absorption saturation and experimental evidence," J. Appl. Phys. **102**, 083101 (2007).
30. R. Philip, G. R. Kumar, N. Sandhyarani, and T. Pradeep, "Picosecond optical nonlinearity in monolayer-protected gold, silver, and gold-silver alloy nanoclusters," Phys. Rev. B **62**, 13160 (2000).
31. U. Gurudas, E. Brooks, D. M. Bubb, S. Heiroth, T. Lippert, and A. Wokaun, "Saturable and reverse saturable absorption in silver nanodots at 532 nm using picosecond laser pulses," J. Appl. Phys. **104**, 073107 (2008).
32. O. Plaksin, Y. Takeda, H. Amekura, N. Kishimoto, and S. Plaksin, "Saturation of nonlinear optical absorption of metal-nanoparticle composites," J. Appl. Phys. **103**, 114302 (2008).
33. R. A. Ganeev, A. I. Ryasnyansky, A. L. Stepanov, and T. Usmanov, "Saturated absorption and reverse saturated absorption of Cu:SiO2 at λ = 532 nm," Phys. Status Solidi (b) **241**, R1–R4 (2004).

1. Introduction

Controlling light beyond the diffraction limit, i.e., at sub-wavelength level, is one of the main challenges of nanophotonics. In particular plasmonic nanostructures with tailored shapes and/or composition are able to produce intense local-field enhancements, which can be further increased by exploiting interaction among the plasmonic nano-building blocks [1–3]. These local-

#156046 - $15.00 USD Received 14 Oct 2011; revised 11 Nov 2011; accepted 13 Nov 2011; published 9 Feb 2012

field enhancement effects are of great interest for example for nonlinear optical applications since they can be effectively exploited to design plasmonic nanosystems with amplified nonlinear optical response [4,5]. From this point of view metal nanoclusters embedded in glasses have attracted much interest over the last decades for their peculiar linear and nonlinear optical properties [6–11]. These are mainly related to the excitation of localized surface plasmon-polaritons (LSPR), with collective oscillations of the free electrons in the metal nanoparticles that give rise to a strong linear absorption band in the visible spectrum, known as surface plasmon resonance (SPR), whose position and intensity depend on the nanocluster size, shape and composition, and on the dielectric properties of the surrounding matrix [3, 12]. Moreover, the local-field enhancement effects that occur in the nanoparticles at SPR wavelengths amplify their nonlinear optical (NLO) response and make these systems very promising for molecular sensing applications and as ultrafast nonlinear optical elements [13–16].

Among the different techniques developed for synthesizing and processing plasmonic nanostructures in insulating matrices, ion implantation/irradiation proved to be a very versatile tool since the functional properties of the nanostructures can be properly tuned by a tailored control of the irradiation parameters [17–20]. Ion irradiation has been effectively employed to produce a peculiar class of nanocluster structures, named "nanoplanets" (NPLs), consisting of a central core cluster surrounded by small satellite clusters [21]. The structural and compositional properties of these systems have been characterized in details as a function of the irradiation conditions, as ion, energy and fluence [22, 23]. The plasmonic properties of the NPLs have also been theoretically investigated in the framework of a full-interaction electromagnetic approach, revealing very large local-field enhancements in the satellite cluster halos [24].

In this work we aimed at linking the near-field properties of Au-Ag bimetallic NPLs to their nonlinear optical properties, experimentally obtained by means of the single beam z-scan technique [25]. For centro-symmetric materials that exhibit NLO response, the refractive index and the absorption coefficient are intensity-dependent and they are commonly written in the form: $n(I) = n_0 + n_2 I$ and $\alpha(I) = \alpha_0 + \beta I$, where n_0 and α_0 are the linear refractive index and absorption coefficient, respectively. The z-scan technique allows to determine the magnitude and sign of both the nonlinear refractive index (n_2) and the nonlinear absorption coefficient (β). The measurements have been performed with a pulsed laser beam in the picoseconds regime in order to avoid thermal effects and to isolate the fast electronic contribution to the optical nonlinearity [26].

2. Experimental

Plasmonic nanoplanets embedded in silica were fabricated following a multiple-ion beam processing technique. Au^+ and Ag^+ sequential ion implantations were performed at room temperature on fused silica (type II, Heraeus) slides with a 200 keV high-current implanter (Danfysik 1090). The current density was maintained at 2 μA/cm^2. Ion energies of 190 keV for Au and 130 keV for Ag were chosen to obtain comparable ion ranges. The fluence was 3×10^{16} ions/cm^2 for both ions. The implanted silica slides were then annealed in air at 800 °C for 1h to promote the bimetallic AuAg cluster formation. Subsequently, Ar irradiations were performed on a set of samples at energy of 190 keV, current density of 0.2 μA/cm^2 and fluence of 2.5×10^{16} ions/cm^2 to induce the nanoplanets formation. In the following the implanted reference sample (i.e., containing just spherical nanoparticles before Ar irradiation) is labeled AuAg, whereas the label AuAg-NPL indicates the Ar-irradiated sample with the formation of NPLs.

Structural and compositional characterizations were performed by transmission electron microscopy (TEM) with a FEI Tecnai F20 field-emission gun (FEG) STEM microscope operating at 200 kV equipped with an EDAX energy-dispersive x-ray spectrometer (EDS). Optical absorption spectra were collected with a JASCO V670 dual beam spectrophotometer in the 300-

#156046 - $15.00 USD Received 14 Oct 2011; revised 11 Nov 2011; accepted 13 Nov 2011; published 9 Feb 2012

800 nm wavelength range.

The nonlinear optical properties of the samples were characterized by z-scan measurements. The basic idea of the z-scan technique is to measure the transmitted intensity as the sample is moved along the propagation direction (z) of a laser beam focused by a converging lens. In this way the intensity on the sample varies as a function of z, being maximum at the lens focus, and the nonlinear effects can be detected as variations in the normalized transmittance. In particular, closed aperture (*CA*) transmittance curves measured through a small aperture are sensitive to phase distortion and are affected by both nonlinear refraction and nonlinear absorption in the samples, whereas open-aperture (*OA*) measurements performed without the aperture carry information only on the nonlinear absorption effects.

The measurements were performed with a ring-cavity, mode-locked Nd:glass laser source. The laser supplies trains of about 100 pulses at a repetition rate of 1 Hz. The single pulse duration is about 6 ps and the time separation between two pulses is 5 ns. A pulse slicer was used in order to select a single pulse out of each train. The laser was operated in the TEM_{00} mode at fixed power output. The laser output was frequency doubled (λ=527 nm) by means of a second harmonic birefringent crystal (β-barium borate, β-BBO). A 100 mm converging lens was used to focus the laser beam. The beam waist w_0 at the focal point was about 20 μm, and the Rayleigh range (diffraction length of the Gaussian laser beam) was z_0=2.7 mm. Closed-aperture and open-aperture transmittance curves were collected simultaneously at each sample position along the beam propagation direction and normalized to a reference signal. For *CA* measurements, an iris diaphragm was used as aperture with a linear transmittance S=0.4. Each point in the z-scan curves is the average of 64 shots. The measurements have been performed at different laser beam intensities obtained by means of optical density filters. The maximum peak intensity was always maintained lower than 1 GW/cm^2 to prevent sample damage or modifications during the scans. A CS_2 reference sample ($n_2 = 3\times10^{-14}$ cm^2/W) was used to calibrate the laser intensity [27].

In the thin-sample approximation $L << z_0$ (L being the sample thickness, about 70 nm in our case) and in the low-intensity regime, the following analytical expression can be used to define the normalized transmittance T through the aperture as a function of the aperture linear transmission S, as shown by Guo *et al.* [28]:

$$T = 1 + \frac{(1-S)^{\mu}\sin\xi}{S(1+x^2)}\Delta\Phi_0 - \frac{1-(1-S)^{\mu}\cos\xi}{S(1+x^2)}\Delta\Psi_0 \tag{1}$$

where

$$\mu = \frac{2\left(x^2+3\right)}{(x^2+9)} \tag{2}$$

$$\xi = -\frac{4x\ln(1-S)}{(x^2+9)} \tag{3}$$

and

$$\Delta\Phi_0 = \frac{2\pi}{\lambda}n_2 I_0 L_e \tag{4}$$

$$\Delta\Psi_0 = \beta I_0 L_e/2\sqrt{2} \tag{5}$$

$x = z/z_0$ is the dimensionless relative position of the sample along the beam propagation direction with respect to the focus of the converging lens. I_0 is the on-axis laser intensity at the lens focus and $L_e = \left[1-\exp^{(-\alpha_0 L)}\right]/\alpha_0$ is the sample effective length, with α_0 the linear absorption coefficient. For open aperture measurements (S=1) Eq. (1) results in the

#156046 - $15.00 USD Received 14 Oct 2011; revised 11 Nov 2011; accepted 13 Nov 2011; published 9 Feb 2012

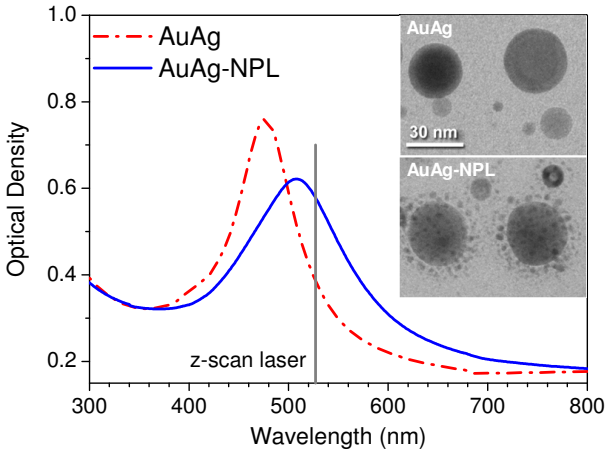

Fig. 1. Optical absorption spectra of the samples with (AuAg-NPL, continuous line) and without (AuAg, dot-dashed line) the nanoplanets. The vertical line indicates the z-scan excitation wavelength. The inset shows the corresponding TEM cross-sectional bright-field micrographs.

conventional expression given by Sheik-Bahae *et al.* [25]:

$$T_{OA} = 1 - \frac{\beta I_0 L_e}{2\sqrt{2}(1+x^2)} \tag{6}$$

In principle, Eq. (1) can be used to obtain both the nonlinear refractive index n_2 and the nonlinear absorption coefficient β. Nonetheless, in order to minimize the number of degrees of freedom and therefore providing a much more reliable determination of the nonlinear parameters we have chosen to fit separately the *OA* and *CA* scans with the Eqs. (6) and (1), respectively, but to get consistent results between the two classes of scans, the fits of the *CA* curves have been always performed by fixing the parameters of the corresponding *OA* fits.

3. Results and discussion

As reported in previous works [22, 23], the sequential implantation of Au^+ and Ag^+ and the subsequent thermal treatments induce the formation in the samples of a population of AuAg alloy clusters with an average diameter of $<D>= 12 \pm 6$ nm, centered at about 60 nm below the silica surface, producing a nanocomposite sub-surface layer of about L=70 nm thickness. The Ar irradiation then promotes the formation of Au-enriched satellite clusters with a mean diameter of about 2 nm at a distance of about 2-3 nm from the original cluster surface, giving rise to the nanoplanets structure. In Fig. 1 we have shown the optical absorption spectrum of these systems (AuAg-NPL, continuous line). The spectrum of the same samples before Ar irradiation, that is previous to the nanoplanets formation, (AuAg, dashed line) is also reported for comparison. The inset shows the corresponding TEM cross-sectional bright-field micrographs. The nanoplanets formation induces a red-shift of the surface plasmon resonance band whose peak shifts from 477 nm (visible in the samples before Ar irradiation) to 508 nm, that is closer to the z-scan excitation wavelength (527 nm). Since the actual composition of the core clusters in the Ar-irradiated samples does not change significantly with respect to the original ones obtained before Ar irradiaton, [23] the changes in the optical spectra cannot be merely interpreted in terms of a compositional change. Conversely, the topological arrangement of the satellites clusters has to be taken into account. Indeed, the observed plasmon shift has been

#156046 - $15.00 USD Received 14 Oct 2011; revised 11 Nov 2011; accepted 13 Nov 2011; published 9 Feb 2012

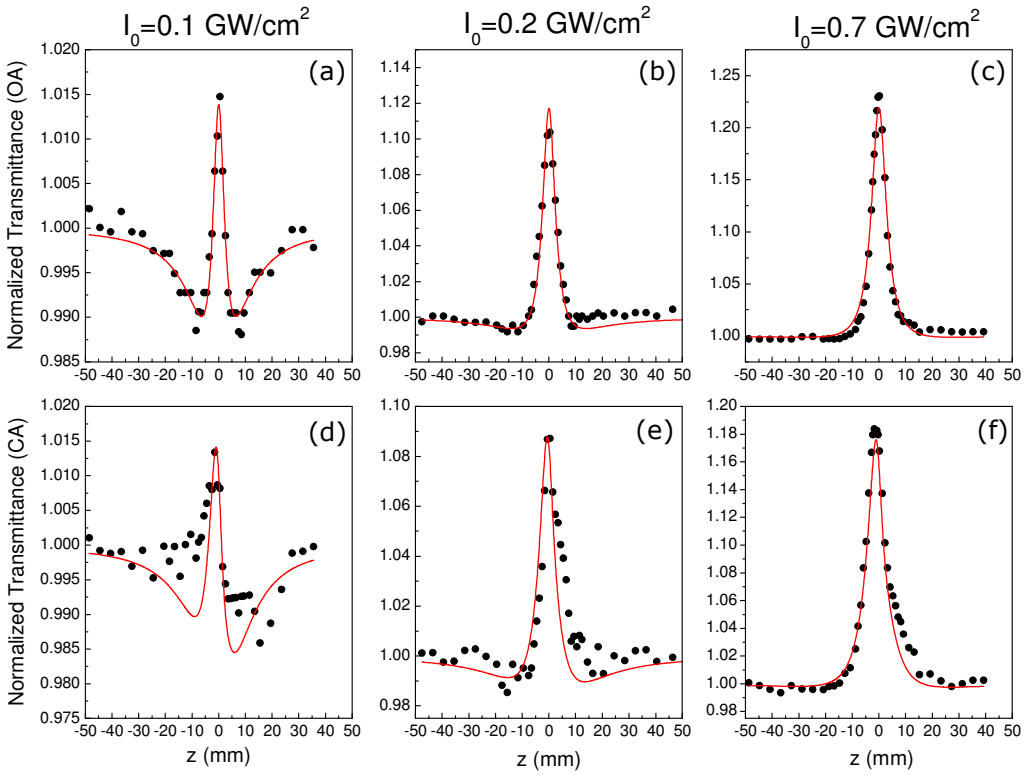

Fig. 2. (a, b, c) open-aperture (*OA*) and (d, e, f) closed-aperture (*CA*) z-scan curves of sample AuAg-NPL, measured at 527 nm at the three indicated laser beam intensities (at the lens focus, I_0). The solid lines represent the best fits according to Eqs. (6) and (1), respectively, following the approach described in the text. The different vertical scales are used to highlight the features visible at the different intensities.

demonstrated to be a consequence of a strong electromagnetic coupling between the core and the satellite nanoclusters, which affects the local-field near the core surface, and local-field enhancements as high as $|\mathbf{E}|/|\mathbf{E}_0| \sim 15$ have been calculated in the satellite cluster halos ($\mathbf{E}_0$ is the incident field) [24].

In Fig. 2 we have reported the open-aperture and closed-aperture z-scan transmittance curves of sample AuAg-NPL measured at three different laser beam intensities in the 0.1-1 GW/cm^2 range. The data are normalized to the linear transmittance measured far from the lens focus. The graphs are plotted with different vertical scales to better highlight the features visible in the different scans. The reproducibility of the results has been checked both for forward and backward scans performed on the same sample position as well as for scans obtained increasing the laser peak intensity up to the maximum value used in this experiment and subsequently decreasing it to its minimum. This ruled out any possible permanent modification of the samples induced by the laser irradiation in the range of intensities explored in this work. At the lowest laser peak intensity the open aperture scan (Fig. 2a) exhibits two opposite features: a transmittance decrease visible in the pre-focal and post-focal regions and a peak in the region close to the lens focus (z=0). This behavior is due to the superposition of two components: a $\beta > 0$ component, responsible for the observed transmittance decrease, induced by reverse saturable absorption phenomena (RSA), and a $\beta < 0$ component giving rise to the central peak, due to

#156046 - $15.00 USD Received 14 Oct 2011; revised 11 Nov 2011; accepted 13 Nov 2011; published 9 Feb 2012

saturable absorption (SA) effects. By increasing the laser peak intensity this SA contribution becomes more and more evident, being completely dominant at the highest intensity (Fig. 2c).

Such effects cannot be accounted for by using a purely constant value of β, as commonly used in the standard z-scan analysis procedure [25], as we will show below. Therefore we assumed an intensity-dependent nonlinear absorption coefficient $\beta(I)$ given by the following expression with two components:

$$\beta(I) = \beta_{RSA}(I) + \beta_{SA}(I) = \frac{\beta_+}{1+\frac{I}{I_s^+}} + \frac{\beta_-}{1+\frac{I}{I_s^-}} \tag{7}$$

where the signs "+" and "-" refer to the RSA (positive) and SA (negative) contributions, respectively. The hyperbolic form has been chosen, as done by Gu *et al.* [29], to introduce a saturation effect at high laser intensities in the nonlinear absorption coefficients. I_s^+ and I_s^- are the corresponding saturation intensities. Consequently, Eqs. (1) and (6) have been corrected by introducing the above expression for the nonlinear absorption coefficient. The solid lines in Fig. 2 are the best fits obtained with this approach. The numerical results are reported in Table 1.

The mechanisms controlling the optical nonlinearity of gold and silver nanoclusters in the picoseconds regime have been investigated in the past by Philip *et al.* studying chemically synthesized AuAg nanoclusters in liquid solutions [30] and more recently by Gurudas *et al.* in pulsed laser deposited Ag nanodots on quartz substrates [31]. In those systems the nonlinear absorption behavior has been explained on the basis of the electron dynamics in the excited states of the metal nanoparticles. According to the authors, for excitation at moderate intensities in the picoseconds time scale, the intraband electron transitions within the conduction band lead to the ground-state plasmon bleaching which results in a SA process. At higher excitation intensities, excited-state absorption related to free carriers becomes significant leading in this case to an RSA process. Moreover, at very high pump intensities even the excited-state absorption responsible for RSA may saturate giving rise in the end to a further changeover to a SA behavior. This last changeover from RSA to SA actually was suggested by the authors, but was not experimentally observed within the pump intensity range available for their work. Conversely, in our samples this evolution is clearly evident already at the minimum laser peak intensity useful for the experiment (Fig. 2a). In fact, due to the intrinsic capability of the z-scan technique to change the intensity on the sample by moving it along the beam propagation direction, the concomitant presence of a RSA ($\beta > 0$) component in the regions far from the lens focus (where the intensity on the sample is the lowest) and a SA ($\beta < 0$) component close to the focus (where the intensity has its peak value in the scan) demonstrates that the RSA towards SA changeover is actually taking place. Then the SA behavior becomes dominant at higher laser peak intensities (Figs. 2b, c). We ascribe the capability to observe this evolution from RSA to SA in our samples already at relatively low laser intensities to the strong local-field enhancement effects induced in the samples as a consequence of the core-satellite coupling in

Table 1. Nonlinear optical parameters measured at 527 nm of the samples with (AuAg-NPL) and without (AuAg) the nanoplanets.

	AuAg-NPL	**AuAg**
n_2 (10^{-10} cm^2/W)	-8 ± 3	-5 ± 1
β_+ (10^{-3} cm/W)	1.9 ± 0.7	0.15 ± 0.03
I_s^+ (10^8 W/cm^2)	0.09 ± 0.04	4 ± 2
β_- (10^{-4} cm/W)	-4 ± 1	-3 ± 1
I_s^- (10^9 W/cm^2)	1.2 ± 0.1	0.010 ± 0.001

#156046 - $15.00 USD Received 14 Oct 2011; revised 11 Nov 2011; accepted 13 Nov 2011; published 9 Feb 2012

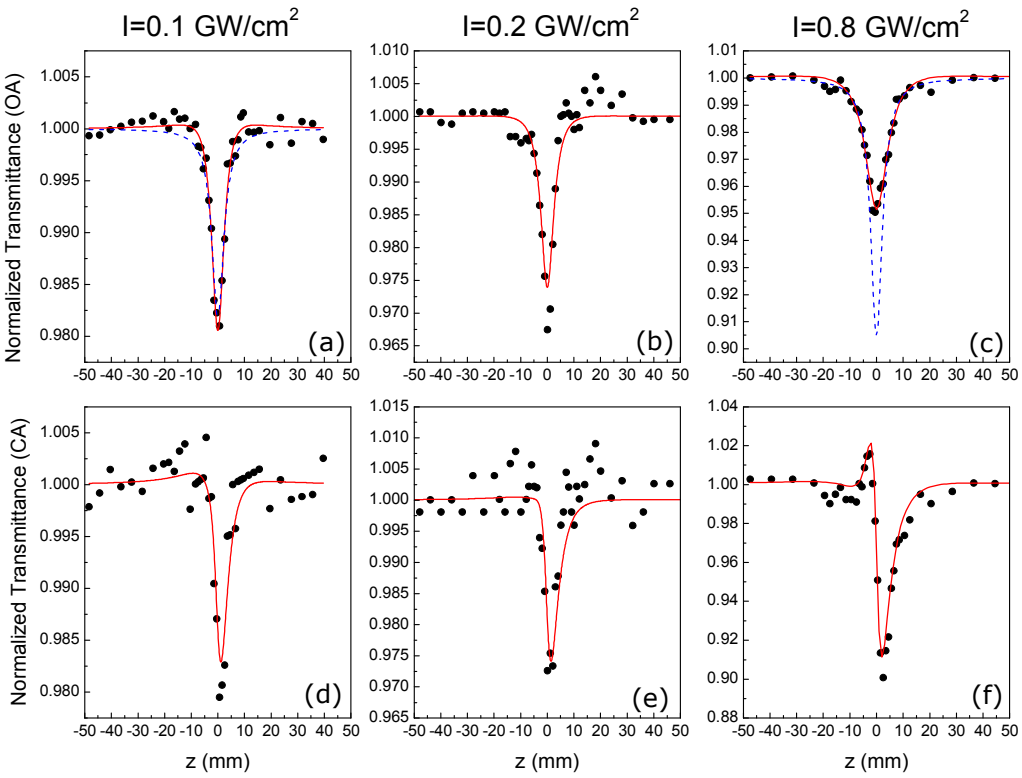

Fig. 3. (a, b, c) open-aperture (*OA*) and (d,e,f) closed-aperture (*CA*) z-scan curves of sample AuAg, measured at 527 nm at the three indicated laser beam intensities (at the lens focus, I_0). The solid lines represent the best fits according to Eqs. (6) and (1), respectively, following the approach described in the text. The dashed lines in (a) and (c) represent the best fit and the simulation, respectively, obtained for an intensity-independent $\beta = 1.1 \times 10^{-4}$ cm/W (see the text for comments).

the nanoplanets. Owing to this, the effective intensity locally experienced by the samples is significantly increased (roughly by two orders of magnitude) with respect to the laser beam intensity.

A validation of this description has been provided by the results of the same z-scan measurements performed on the non-irradiated samples (AuAg). As previously mentioned, indeed, these systems are analogous to the Ar-irradiated ones (containing the nanoplanets) from a compositional point of view. Conversely, they exhibit a blue-shifted SPR band out of resonance with the z-scan laser excitation wavelength and therefore much lower field enhancement factors. For this reason these samples are the most suitable to check the effect on the nonlinear optical properties of much lower effective intensities experienced by the samples. To this aim, we have performed z-scan measurements on AuAg samples in the same intensity range explored to investigate those containing the nanoplanets (AuAg-NPL). The experimental results are reported in Fig. 3. The main feature that can be observed in the *OA* scans of these samples is a transmittance decrease as the sample approaches the lens focus induced by RSA processes. This behavior is visible at all the investigated laser peak intensities. Consistently, also in this case the z-scans have been analyzed by introducing an intensity-dependent nonlinear absorption coefficient, given by Eq. (7), following the same procedure used to analyze the AuAg-NPL

#156046 - $15.00 USD Received 14 Oct 2011; revised 11 Nov 2011; accepted 13 Nov 2011; published 9 Feb 2012

sample. The solid lines in Fig. 3 are the best fits obtained in this way. The numerical results are also summarized in Table 1.

To better support the scheme adopted, we compared the present analysis with the standard one [25] that assumes a constant value of the nonlinear absorption coefficient β in Eq. (6). The results are shown in Fig. 3a, c with dashed lines: although a reasonably good fit is obtained at low intensity (Fig. 3a, dashed line), a simulation of the expected *OA* curve at high laser peak intensity with this value of β (Fig. 3c, dashed line) demonstrates that the simple picture of a constant β value fails to describe the experimental results in the whole intensity range. As shown, in this case the experimental *OA* scan exhibits a much less pronounced minimum at the lens focus with respect to the simulation, suggesting a lower (i.e., not constant) nonlinear absorption coefficient. It is worth noting that a better level of agreement with the experimental *OA* data could be obtained with this constant value of β if the Rayleigh range z_0 is treated as a free parameter in the fitting procedure. Nonetheless this would lead to an inconsistent increase of the value of z_0 as the laser peak intensity is increased, which is unphysical since z_0 is independent of the beam intensity and it is defined only by the given experimental set-up [32]. These results thus demonstrated that in our samples: (i) the nonlinear absorption coefficient β is a function of the laser intensity and (ii) at the highest intensities in the range explored the excited-state absorption processes, responsible for the RSA behavior, saturate. Moreover, by introducing a SA component (β_{SA}) in the nonlinear absorption coefficient (Eq. 7) it has been possible to account also for the small humps visible in the pre-focal and post-focal region in the low intensity *OA* scan (Fig. 3a). For these samples therefore the nonlinear absorption behavior is characterized by a changeover from SA exhibited at very low intensities towards RSA at moderate intensities that in turn further saturates at the maximum intensities accessible for the experiment. It is worth underlining that the whole nonlinear behavior so-far described is consistent with the mechanism proposed by Philip *et al.* [30] to describe the picosecond nonlinear properties of 3-4 nm Au or Ag nanoparticles in solutions and with the results by Ganeev *et al.* on 4 nm Cu nanoparticles in silica [33].

Figure 4 summarizes the evolution of the nonlinear absorption coefficient $\beta(I)$ as a continuous function of the intensity in the two samples, as computed with the data reported in Table 1. The overall opposite behavior is evident in the two samples: at high intensities the saturating SA component dominates in the AuAg-NPL sample whereas the saturating RSA one is the most effective in the AuAg. Of course what is important from an applicative point of view is the product βI, which is the nonlinear correction to the linear absorption coefficient α_0. This implies that in Fig. 4 the high-intensity side of the curves is dominating. To investigate this point we plotted in Fig. 5 the resulting values of the normalized intensity-dependent absorption coefficient $\alpha(I)/\alpha_0$ as a function of the laser intensity. AuAg sample behaves as an optical limiter, i.e., its $\alpha(I)$ increases at high laser intensities, whereas AuAg-NPL sample exhibits a decreasing value of absorption as I is increased. It is interesting to note that in this last case for laser intensities close to 1 GW/cm^2 the normalized absorption approaches zero and eventually could become negative (if extrapolating the measured data at higher intensities), therefore behaving like an effectively optical gain material. Unfortunately this range of intensities is not experimentally accessible since it is beyond the damage threshold for these materials, above which we observed permanent modifications of the samples that completely alter their optical response. This limitation could be overcome through a further optimization of the local-field enhancement properties of the plasmonic nanostructures (either nanoplanets or more complex architectures), which could make the optical gain regime already accessible at laser intensities below the damage threshold.

A final comment on the value of the nonlinear refractive index n_2 is worth doing. As it can be seen in Table 1, although the β values differ substantially (both in sign and magnitude) in

#156046 - $15.00 USD Received 14 Oct 2011; revised 11 Nov 2011; accepted 13 Nov 2011; published 9 Feb 2012

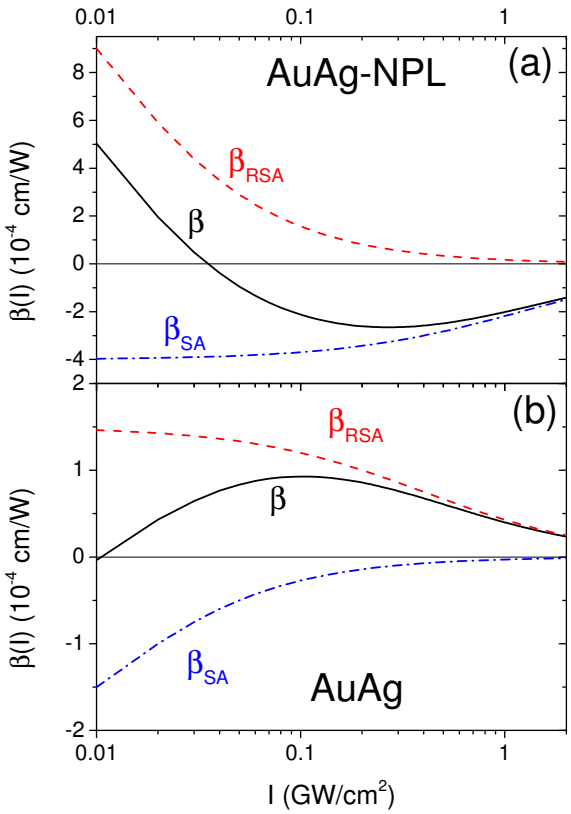

Fig. 4. Evolution of the nonlinear absorption coefficient β (solid line) and of its components β_{RSA} (dashed line) and β_{SA} (dot-dashed line) plotted as continuous functions, obtained from the NLO data measured at 527 nm as a function of the laser intensity for AuAg-NPL sample (a) and for the AuAg sample (b).

the AuAg and AuAg-NPL samples, their n_2 values measured by z-scan are of the same order of magnitude (and comparable with similar samples as in ref. [14]) and intensity-independent. This can be consistently interpreted by considering that from a topological point of view the difference in the scattering cross section between AuAg-NPL and AuAg nanoparticles is mainly controlled by the halo of satellites whose size is about 2 nm. In this size range, the dipolar approximation can be used in the visible range (i.e., the cluster radius R is much smaller than the wavelength of light λ) and therefore the extinction cross section (i.e., the sum of scattering and absorption cross sections) results to be mainly controlled by the absorptive part (proportional in the dipolar approximation to R^3), whereas the scattering cross section, being proportional to R^6, is almost negligible. Therefore from a scattering point of view the satellites halo is equivalent to an effective medium shell layer that changes locally the dielectric environment of the core nanoparticles, resulting in a net red-shift of the cross sections without altering too much the contribution of the scattering with respect to the absorption component. For this reason in the far field we can expect the larger effect of the nonlinear coefficient in the absorption part, and not in the scattering (refractive) part, in agreement with the present results.

#156046 - $15.00 USD Received 14 Oct 2011; revised 11 Nov 2011; accepted 13 Nov 2011; published 9 Feb 2012

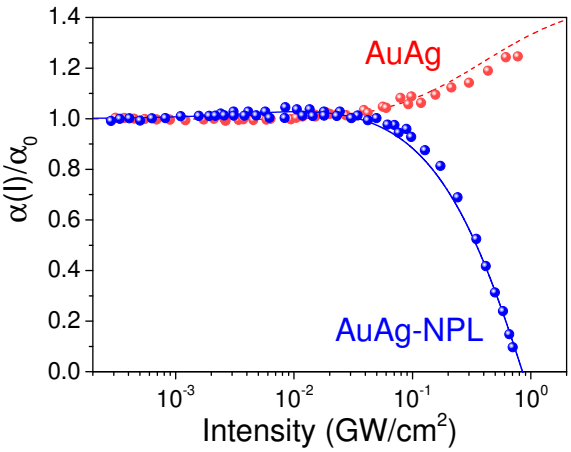

Fig. 5. Evolution of the normalized absorption coefficient $\alpha(I)/\alpha_0$ measured at 527 nm as a function of the laser intensity for AuAg and the AuAg-NPL samples: dots represent experimental points from the z-scans in the whole intensity range and the lines are the functions computed with the measured values reported in Table 1

4. Conclusions

In this work, the nonlinear optical properties of Au-Ag nanoplanets have been experimentally investigated close to their surface plasmon resonance by means of the single beam z-scan technique. The measurements have been performed in the picoseconds regime in order to isolate the fast electronic contribution to the optical nonlinearity. The results reveal that both AuAg nanoplanets and AuAg nanoparticles exhibit large values of the nonlinear optical parameters with an opposite sign of the (intensity dependent) nonlinear absorption coefficient, demonstrating that at the highest intensities investigated (below the damage threshold) AuAg nanoplanets behave as a saturable absorber, whereas AuAg nanoparticles exhibit an optical limiting character. On the other hand, our experimental results allowed to reveal in the AuAg nanoplanets the peculiar strong local-field enhancement effects, theoretically expected considering the core-satellite coupling. As an important consequence, this enabled to investigate nonlinear phenomena that could not be activated even at the highest excitation intensities in the sample without nanoplanets. Finally, we found in the nanoplanet configuration a dramatic decrease of the absorption coefficient, which approaches zero at intensities close to the threshold for sample damage. This prompts for the design of optimized plasmonic nanostructures whose local-field enhancement properties could make this optical gain regime already accessible at laser intensities below the damage threshold.

Acknowledgments

This work was partially supported by the University of Padova (Italy) through the strategic project PLATFORMS (STPD089KSC).

#156046 - $15.00 USD Received 14 Oct 2011; revised 11 Nov 2011; accepted 13 Nov 2011; published 9 Feb 2012